

Topological scaling and gap filling at crisis

K. Gábor Szabó,^{1,2} Ying-Cheng Lai,³ Tamás Tél,² and Celso Grebogi⁴

¹Department of Mathematics, University of Kansas, Lawrence, Kansas 66045

²Institute for Theoretical Physics, Eötvös University, P.O. Box 32, Budapest, H-1518, Hungary

³Department of Mathematics and Department of Electrical Engineering, Arizona State University, Tempe, Arizona 85287

⁴Institute for Plasma Research, Department of Mathematics, and Institute for Physical Science and Technology, University of Maryland, College Park, Maryland 20742

(Received 16 December 1998; revised manuscript received 18 October 1999)

Scaling laws associated with an interior crisis of chaotic dynamical systems are studied. We argue that open gaps of the chaotic set become densely filled at the crisis due to the sudden appearance of unstable periodic orbits with extremely long periods. We formulate a scaling theory for the associated growth of the topological entropy.

PACS number(s): 05.45.Ac

I. INTRODUCTION

The behavior of a physical system is usually determined by one or more invariant sets in its phase space. As system parameters vary, qualitative changes in the invariant sets can occur, leading to physically observable phenomena. An *interior crisis* [1] is such a qualitative change that occurs in dissipative nonlinear systems, in the phase space of which an attracting set coexists with a nonattracting chaotic set. As the system parameters change, the attractor can collide with the coexisting nonattracting chaotic set that leads to a sudden enlargement of the chaotic attractor. Interior crises have been observed in many experiments [2,3].

A scaling law describing the growth of the topological entropy at interior crises was presented in Ref. [4]. We found that for some system parameter a the topological entropy h obeys the algebraic scaling law

$$h(a) - h(a_c) \sim (a - a_c)^\chi \quad \text{with } \chi = h(a_c)/\Lambda \quad (1)$$

beyond the crisis value a_c , where χ is the *gap filling exponent* and Λ denotes the Lyapunov exponent of the unstable periodic orbit mediating the crisis.

In the present paper, on the one hand, we demonstrate how an interior crisis triggers the creation of new unstable periodic orbits, and analyze how the emergence of infinitely many periodic points leads to the sudden and complete filling of formerly empty, dense regions of the phase space (*gap filling*). We emphasize the crucial role of the mediating orbit in this process. On the other hand, we refine the conditions, elaborate the derivation of Eq. (1), and present refined estimates of the theory with a special focus on the details of the diagram technique being used. We also provide further supporting numerical results, and comment on the common fine scale behavior of scaling quantities at interior crisis.

The paper is organized as follows. In Sec. II we describe the phenomenon of interior crisis, study the geometric structure of the phase space for parameter values around the crisis, and introduce the notation. In Sec. III we investigate the dynamics of the coupling orbits, which is a key step toward the understanding and the derivation of scaling law (1) for the topological entropy. In Sec. IV we derive our main result, the scaling law (1). We present numerical results in Sec. V

and discussions in Sec. VI. Some details of the diagram technique are left for the Appendix.

II. PHASE-SPACE STRUCTURE AT INTERIOR CRISES

A. Notions and definitions

Consider a dissipative dynamical system described by the map

$$\mathbf{x}_{n+1} = \mathbf{F}(\mathbf{x}_n, a), \quad (2)$$

where $\mathbf{x} \in \mathbb{R}^N$, and a is a system parameter that can be varied. We consider a parameter regime where the system exhibits chaos with one positive Lyapunov exponent, i.e., we exclude the possibility of hyperchaos. We assume that the system is smooth, so that the periodic orbits and the invariant manifolds change continuously with the parameter. A chaotic attractor of the system is in the closure of the unstable manifolds of the periodic orbits embedded in the attractor. The parameter regions where such an attractor exists and produces sustained chaos are interrupted by periodic windows. In this subsection we outline the general mechanism of interior crisis in typical periodic windows. We refer the reader to Fig. 1 for a schematic picture of the phase-space development of the invariant sets involved.

A periodic window occurs due to the creation of a stable-unstable pair of period p orbits by a saddle-node bifurcation. Beyond the bifurcation parameter value a_b the stable orbit has a primary basin of attraction bounded by the codimension-1 stable manifold of its accompanying unstable orbit. As the parameter changes the stable orbit undergoes period doubling and evolves into a small chaotic attractor. The chaotic attractor gradually grows within its basin of attraction, until it eventually collides to its basin boundary at the critical value a_c . On a bifurcation diagram this small attractor appears in p bands, since its basin of attraction consists of p pieces in the phase space. Therefore, we refer to the primary basin of attraction as the *band region* (B), and its complement as the *surrounding region* (S).

The chaotic attractor loses its asymptotic stability when it collides with the basin boundary of region B at some parameter value $a_* \geq a_b$, and transforms to a chaotic saddle [5]. Between a_* and a_c the chaotic saddle is located in region S , and coexists with the (usually small) attractor residing in the

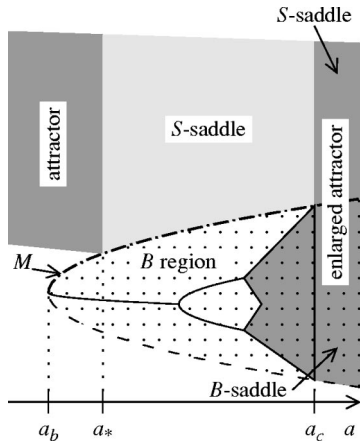


FIG. 1. The structure of the invariant sets in a typical periodic window. The (dotted) band (B) region is bounded by the mediating periodic orbit M (dash-dotted line) and its stable manifold (dashed line). Within the window, $a_b < a < a_c$; this is the primary basin of attraction of the p piece attractor. Meanwhile, at $a_* \geq a_b$, the chaotic invariant set in the complementary surrounding (S) region loses its stability and becomes a chaotic saddle (S saddle). Beyond the crisis a_c , both *basic components*, the B saddle within the band region and the S saddle within the S region, are nonattracting chaotic sets *embedded* in the enlarged chaotic attractor.

band region B . Since every periodic orbit is restricted exclusively either to B or S , it is possible to split the whole chaotic set into two *basic components* that we define here as the nonwandering sets within the B and S regions, respectively. The dynamical nature of the basic components (and the associated chaotic behaviors) are very distinctive: in addition to the obvious difference between their transient and permanent temporal character, they usually also differ in other quantitative characteristics like amplitude, Lyapunov exponent, frequency spectrum, etc.

As a passes through the critical value a_c , an attractor enlargement occurs: the chaotic attractor collides with the chaotic saddle and loses its asymptotical stability. The collision of the basic components occurs at an unstable periodic orbit M [1], which “mediates” the crisis. The *mediating orbit* has a period of p (or the integer multiple thereof) and a codimension-1 stable manifold that forms the boundary [6] between the B and S regions.

Beyond the crisis point, a trajectory can penetrate the boundary between B and S both ways; thus it typically keeps switching back and forth between the two phases, a behavior known as *crisis induced intermittency* [7]. In this parameter regime a sequence of trajectory points that fall in the surrounding region is called a *burst* [1]. The dynamical characteristics of the bursts are clearly distinguishable from those of the other phase of the motion spent in region B , as these are inherited from those of the basic components before the crisis. The above definition of the basic components (e.g., being the nonwandering sets of B and S regions separated by the stable manifold of M) can be naturally extended to the postcritical parameter regime too.

As we demonstrate in Sec. III, whenever a trajectory penetrates the boundary from B to S , it approaches the mediating orbit M along its stable manifold and then leaves it along its unstable manifold. While staying in one of the S or B regions, the respective basic component imposes its own dy-

namics on the trajectory. While staying in the close vicinity of M , the trajectory follows the mediating orbit’s pattern; therefore, it is practically the same in every such event. The evolution of a typical trajectory in the postcritical regime thus follows the scenario:

$$\begin{aligned} (\text{chaos})_1 &\rightarrow (\text{approximately periodic}) \rightarrow (\text{chaos})_2 \rightarrow (\text{chaos})_1 \\ &\rightarrow (\text{approximately periodic}) \rightarrow (\text{chaos})_2 \rightarrow (\text{chaos})_1 \\ &\rightarrow \dots \end{aligned} \quad (3)$$

The above scheme amends the one set forth in Ref. [7], and provides us with a one-to-one correspondence between the basic components and the typical chaotic signals. The escape rates of the basic nonattracting sets determine the characteristic time scale of the respective typical signals [8,1].

In experiments it is often possible to make a reliable distinction between typical signals. In such cases we can use the above correspondence to determine the dynamical characteristics from the measurement data. In addition to various techniques developed to measure the lifetime, various dimensions, and entropies, it is also possible to use phase space reconstruction to locate and separate the basic components [3].

In what follows, we give two examples, one- and two-dimensional maps, where the mediating orbit, its stable manifold, the S and B regions, and the basic components within them can be determined by analytic or numeric methods. Note that both our examples are strongly dissipative systems, where a_b and a_* coincide [1], and the mediating orbit M is actually the same unstable orbit that is created by the saddle-node bifurcation at $a = a_b$.

B. Example 1: Quadratic map

As the first example we consider the main period-3 window of the one-dimensional quadratic map,

$$x_{n+1} = f(x_n) = a - x_n^2, \quad (4)$$

on the interval $|x| < |1 + (4a + 1)^{1/2}|/2$. The period-3 window lies in the parameter interval $a_b = a_* = 1.75 < a < a_c = 1.79032749199\dots$ [1]. The unstable period-3 orbit $M \equiv \{x_a, x_b, x_c\}$ is generated by the saddle-node bifurcation at $a = a_b$. The interior crisis (attractor enlargement) occurs at a_c . Figure 2 shows the mapping and the location of the basic components close to this parameter value.

Somewhat before the crisis the three piece region $B \equiv B_1 \cup B_2 \cup B_3$ is mapped *into* itself, thus forming the primary basin of attraction of a three piece attractor. On the other hand, the map restricted to $S \equiv S_1 \cup S_2$ is not closed: since S is mapped *onto* $S_1 \cup B_1 \cup S_2$, almost all trajectories started from S sooner or later leave that region and are trapped in B . However, there exist an infinite number of periodic and aperiodic orbits in S which never escape from this region. These orbits form another invariant set within S , which is asymptotically unstable, notwithstanding chaotic [9]: a chaotic repeller. The repeller has a Cantor set structure, and it can be constructed by a recursive procedure discussed in detail in Ref. [10]. The boundary between the two regions is formed by the periodic orbit M and some of its preimage points x_A , x_B , and x_C . As the parameter is changed, at a

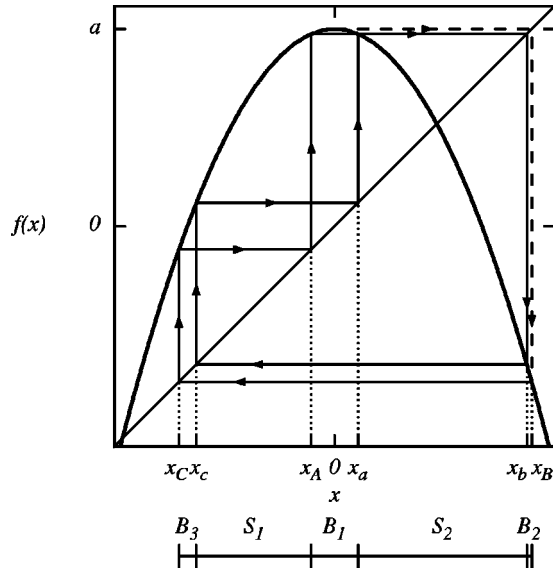


FIG. 2. The quadratic map about the attractor enlargement crisis. The mediating period-3 orbit (x_a, x_b, x_c) and the points x_A , x_C , and x_B determine the end points of the B and S intervals. The arrows indicate how they are mapped onto each other. The broken line shows how the apex point is mapped forward: either into B_2 , exactly on x_B , or outside of B_2 , depending on the actual parameter value.

$=a_c$, the maximum point is just mapped on x_B (see Fig. 2); thus the three piece chaotic attractor covers the whole primary basin of attraction (B) and touches the neighboring repeller at the boundary points.

For parameter values beyond the crisis value a_c , the maximum point is mapped *outside* B_2 , cf. Fig. 2. Thus the map restricted to region B is not closed any longer, and the chaotic attractor undergoes a sudden enlargement: it becomes a one piece attractor by extending to the whole interval $A \equiv [f(a), a]$. After the crisis, however, it is still possible to identify the former chaotic sets. Orbits that never leave the region S form again a Cantor set repeller that can be constructed the very same way as before. Analogously, it is also possible to construct the set consisting of orbits that never escape from the band region, yielding another Cantor set structure [10]. Both basic components are repellers embedded in the large attractor A .

A major advantage of this example is that the topological entropies of the basic components can be calculated exactly [10]:

$$h^{[B]} = \log(2)/3 \quad \text{for } a > a_c, \tag{5}$$

$$h^{[S]} = \log[(1 + \sqrt{5})/2] \quad \text{for } a > a_b.$$

The fact that the topological entropy is constant reflects very strong structural stability. Indeed, the repeller in S does not change topologically while the system goes through the crisis. Beyond the crisis both basic component repellers become structurally stable.

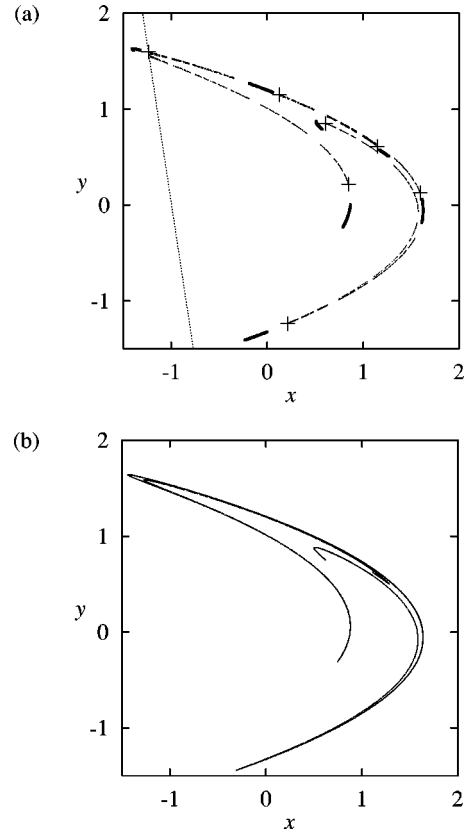


FIG. 3. (a) The chaotic invariant sets of the Hénon map at $a = 1.266 < a_c$, inside the period-7 window. A chaotic saddle (light dots) coexists with the seven piece chaotic attractor (heavy dots). The mediating period-7 points (+) and the tangent to the stable manifold of one of them (dotted line) are also shown. (b) The enlarged Hénon attractor $a = 1.276 > a_c$ beyond the period 7 window.

C. Example 2: Hénon map

While the basic chaotic invariant sets can be characterized analytically for one-dimensional maps, in two dimensions one resorts to numerical computations. We consider the Hénon map [11]

$$(x_{n+1}, y_{n+1}) \mapsto (a - x_n^2 + 0.3y_n, x_n), \tag{6}$$

close to $a_c = 1.271\,685\,6\dots$, where an interior crisis occurs in a period-7 window.

Below this critical value the chaotic attractor is located in seven well separated bands in the phase space, as shown in Fig. 3(a) together with the period-7 hyperbolic orbit mediating the crisis. There is a visible distance between the attractor and the mediating points which gradually disappears as the parameter approaches a_c ; then the attractor collides with its basin boundary at this orbit. The basin boundary of the attractor is formed by the branches of the stable manifold of the mediating orbit. Locally, these can be approximated by their tangent lines along the stable eigendirections of the mediating points. In Fig. 3(a) we also show one of these lines. The tangent approximations of the stable manifolds can be utilized as numerical criteria for the basin boundary. This was used to find a numerical approximation of the coexisting chaotic saddle in the surrounding region. (The numerical procedure was outlined in Ref. [6].) Note that, in an analogy to the one-dimensional example, the chaotic saddle

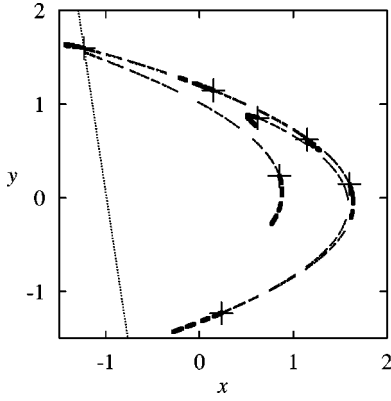


FIG. 4. The basic components of the Hénon map at the same parameter values as used in Fig. 3(b): the B saddle (heavy dots) and the S saddle (light dots). Both chaotic saddles exhibit pronounced fractal structures along their unstable manifolds. The period-7 orbit (+) mediates between the two basic components. The dotted line is the same tangent shown in Fig. 3(a).

also has a Cantor-set-like fractal structure with finite size gaps along its unstable foliation [Fig. 3(a)].

As the parameter passes through a_c , the chaotic attractor abruptly extends so as to form a single, continuous set along its unstable foliation [Fig. 3(b)]. Embedded in the attractor lies the remnant of the precritical seven piece attractor and the continuation of the precritical saddle. We obtained the two basic components numerically by the same method as before; the result is shown in Fig. 4. Apparently, the component in S does not differ from the precritical chaotic saddle [c.f. Fig. 3(a)]. We have also found numerically (see Sec. V) that its topological entropy is constant through a_c . This supports our view that these chaotic saddles are typically structurally stable at crises and, therefore, can be used as building blocks of the whole chaotic set. Comparing Figs. 3(a) and 4, note that the basic component in the band region also develops a fractal structure when it becomes nonattracting after the crisis.

D. Gap filling

The above paradigmatic examples demonstrate some general topological features at internal crises. The S -saddle component has a fractal structure along the unstable foliation leaving *an infinite number of finite size gaps* in between. The S saddle is a structurally stable set; it is topologically unchanged throughout the crisis and throughout most of the periodic window. Before the crisis these gaps are left empty. After the crisis, however, since the leaving from and reentering to region S becomes topologically permitted, periodic points that are not part of the nonwandering sets appear both in S and B . This infinitesimally small change in the parameter at a_c generates uncountably many periodic points of this kind which abruptly *fill in all the gaps* of the S saddle, completely and densely along the unstable foliation. (The first experimental observation of this phenomenon was reported, but not analyzed, in Ref. [12].)

These orbits establish the dynamical connection between the basic components, via a complex chain of homoclinic and heteroclinic crossings of stable and unstable manifolds [13]. Therefore, we call them *coupling orbits*, and the new

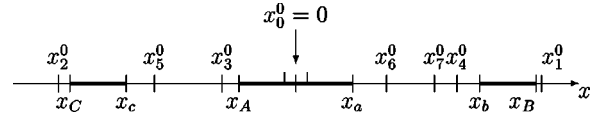


FIG. 5. The mechanism of postcritical intermittency in the quadratic map.

component of the chaotic set they form the *heteroclinic component*. The coupling orbits from the “bulk” of the chaotic attractor and they play a crucial role in the structural development of the chaotic set beyond the crisis. However, as we shall point out, the heteroclinic component is structurally volatile and, as the scheme (3) and Figs. 3(a) and 4 suggest, in fact the robust basic components do serve as *dynamical* as well as *geometrical frameworks* of the system.

III. ANATOMY OF THE COUPLING ORBITS

To describe the gap filling phenomenon, quantitatively, it is necessary to study the dynamics of the newly created coupling orbits after the crisis. The coupling orbits visit both regions B and S for $a \geq a_c$. Let $m(a)$ be the *minimum length* of these orbits. We found [4] that $m(a)$ diverges logarithmically:

$$m(a) \propto -\log(a - a_c). \quad (7)$$

Equivalently, for every natural number m one can assign threshold parameter values a_m , below which coupling orbits of length less than m do not exist. From Eq. (7) we see that the sequence a_m must approach the critical value a_c as a geometrical sequence:

$$a_m - a_c \approx \text{const } e^{-\Lambda m}, \quad (8)$$

where Λ is the positive local Lyapunov exponent of the mediating orbit taken at crisis. First, in Sec. III A, we demonstrate this proposition on the example of the period-3 window of the quadratic map (4). We defer the generalization to Sec. III B.

A. Self-similarity of coupling orbits in a one-dimensional map

Consider $\{y_i\}_{i \in 1, \dots, m}$, (one of) the shortest coupling orbits at a given postcritical parameter value a with length m . This orbit stays in region B (of the precritical attractor), from where it escapes after a while and enters to region S (of the precritical repeller), then finally returns to B again (cf. Fig. 2). Since it is the shortest orbit, it cannot do this loop more than once. We choose $y_0 \equiv y_m$ to be the last point before escaping the region B : it lies within B_1 very close to the apex point 0. Let x_i^0 be $f^{(i)}(0)$, the i th image of the apex point. From Figs. 2 and 5 we see that the first point after escape, y_1 , falls into the *escape interval* $[x_B, x_1^0]$, and after three additional steps the fourth iterate is very close to the mediating period-3 orbit: $y_4 \in [x_a, x_b]$, already inside region S . The following points of the orbit must lie in the subsequent images of the escape interval: $y_5 \in [x_c, x_5^0]$, $y_6 \in [x_a, x_6^0]$, $y_7 \in [x_7, x_b], \dots$, $y_{3l} \in [x_a, x_{3l}^0]$, $y_{3l+1} \in [x_{3l+1}, x_b]$, $y_{3l+2} \in [x_c, x_{3l+2}^0], \dots$, etc., until the iteration leads back to the initial point $y_m = y_0 \approx 0$.

Note that, close to the crisis, the length of the first interval

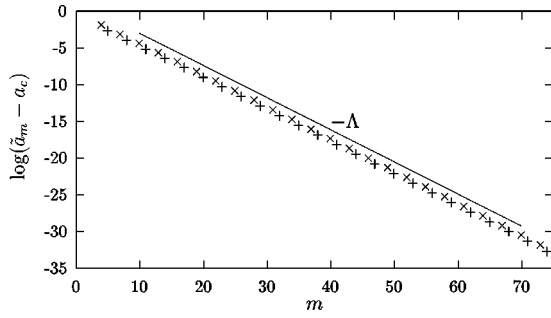


FIG. 6. \times and $+$ marks show the superstability points \tilde{a}_m of the shortest coupling orbits of the $m=3l+1$ and $m=3l+2$ families, respectively. Both series of data points fit to straight lines of slope $-0.437 = -\Lambda$ on a semilogarithmic scale (of base e).

$[x_B, x_1^0]$ is approximately *proportional to the excess parameter value* $a - a_c$, and so is that of the fourth, $[x_4^0, x_b]$:

$$x_b(a) - x_4^0(a) \propto a - a_c. \tag{9}$$

It follows then that the studied orbit, and likewise *every coupling orbit, draws very close to the mediating orbit* right after escaping from B as $a \rightarrow a_c$. Consequently, it spends a considerable time in the vicinity of the mediating orbit, in a sort of intermittent phase of the motion. During this period the trajectories are subjected to the repulsion of the unstable mediating period-3 orbit, and are driven away exponentially with the rate determined by its local Lyapunov exponent Λ , e.g.,

$$\frac{x_b - y_{3l+4}}{x_b - y_{3l+1}} \approx \frac{x_b - x_{3l+4}}{x_b - x_{3l+1}} \approx f^{(3)'}(x_b) = e^{3\Lambda}. \tag{10}$$

The periodic orbit $\{y_1, \dots, y_m\}$ cannot return to the vicinity of 0 before the image of the original escape interval extends to the size of the whole region, which is of magnitude 1. From Eq. (10), this latter condition can be written as

$$x_b - y_m \approx 1 \propto e^{(m-4)\Lambda} (x_b - x_4^0). \tag{11}$$

This, in combination with Eq. (9), leads to Eqs. (7) and (8) for large m values.

Figure 6 shows the result of the numerical calculation which reflects the scaling relation (8). In particular, we examine parameter value \tilde{a}_m at which the shortest periodic orbits are just superstable ($y_0 = y_m = 0$). These parameter values are extremely close to the births of the orbits a_m , and should exhibit the same scaling law. Both \tilde{a}_{3l+1} and \tilde{a}_{3l+2} as a function of m fit in a logarithmic representation to a straight line of slope -0.437 in agreement with our expectation, since the value of the Lyapunov exponent of the mediating orbit at crisis is $\Lambda = 0.437452 \dots$. (We note that the series \tilde{a}_{3l} , obtained as the superstability points of the shortest period $3l$ coupling orbit, behaves similarly; however, it can be shown that the period of the shortest possible coupling orbit is never divisible by 3.)

Thus, for the quadratic map (4), scheme (3) provides an adequate model of crisis induced intermittency. Let us introduce the following symbolic representation of the chaotic behavior:

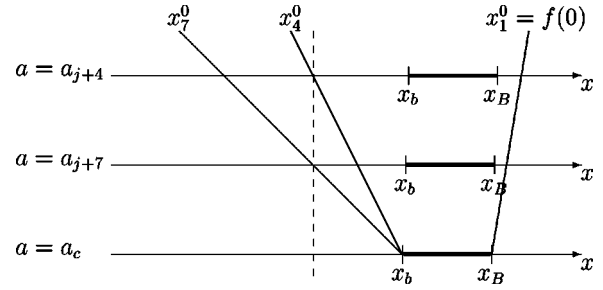
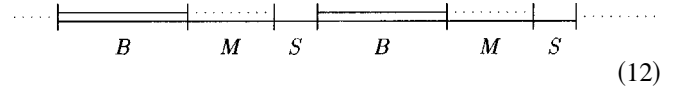


FIG. 7. Schematic illustration of topologically analogous situations in a one-dimensional map. The dashed line shows the position of the j th preimage of a special point of the map. The mediating point is x_b .



where double lines symbolize $(\text{chaos})_1$, the dominant behavior within region B ; single lines, $(\text{chaos})_2$, the chaos within S during a burst; and the dotted single line represents the intermittent motion close to the mediating period-3 orbit M . This pattern is valid in the whole postcritical regime, but, according to Eq. (7), the minimum length of the intermittent phase diverges as the crisis point is approached from above.

Note that the data in Fig. 6 belonging to the period $3l+1$ and $3l+2$ orbits fit to two different lines. This suggests that similar situations occur for periodic orbits belonging to the same line. We call these situations *topologically analogous*, and we say that the sets of superstability points $\{\tilde{a}_{3l+1}\}$ and $\{\tilde{a}_{3l+2}\}$ form two *families* of topologically analogous situations.

Figure 7 illustrates the essence of this similarity, and the mechanism by which these topologically analogous situations recur as the system parameter is varied. Let the dashed line represent the position of the j th preimage of the apex point. At $a = \tilde{a}_{j+4}$ the fourth image of 0 falls exactly onto this position; thus it returns to 0 after j subsequent iterations. While approaching a_c , the width of the interval $[x_4^0, x_b]$, accessible by the fourth step after the escape, decreases proportionally to $a - a_c$. If the excess parameter value $a - a_c$ is decreased by a factor of being approximately $e^{-3\Lambda}$, then the apex point is mapped again on the j th preimage of itself (thus becoming superstable again); however, this requires three more iterations in this case.

Figure 7 thus implies that for subsequent members of a family of topologically analogous situations, the relation

$$\frac{\tilde{a}_{m+3} - a_c}{\tilde{a}_m - a_c} \approx e^{-3\Lambda} \tag{13}$$

holds. This indeed implies an asymptotically geometrical convergence with the same quotient as the one for a_m 's, the appearance of shortest coupling orbits, in Eq. (8).

In addition to the superstable situations, topological similarities can also be found among situations where the apex point of the parabola is mapped onto a periodic orbit after a finite number of iterations. Such a situation is called a *Misiurewicz point* [14]. Figure 7 also illustrates this more general case: the dashed line now denotes the j th preimage of an arbitrary periodic point. Those Misiurewicz points, where the

origin is mapped onto a well defined preimage of a given fixed point, can be gathered into families of topologically analogous situations, similarly to the (three) families of superstability points \tilde{a}_{3l+i} ($i=1,2,3$). There are, of course, infinitely many of such families. The members of a family of Misiurewicz points satisfy the same scaling relation (13) for the superstable points and the birth points of the shortest coupling orbits.

The existence of these topologically analogous situations is a consequence of the *self-similar* behavior in the vicinity of the crisis point. Self-similarity is a general sign of critical behavior. Therefore, we conjecture that, in addition to the special situations discussed above, arbitrary situations at general system parameter values can be gathered into families of topologically analogous situations. All of these families asymptotically follow Eq. (8) with the same scaling exponent 3Λ . The constant coefficient in Eq. (8), however, differs from family to family.

B. Generalization

The mechanism outlined above is restricted neither to the quadratic map (4) nor to its period-3 window. By making appropriate changes according to the actual orbits being involved, the above arguments work for every interior crisis of any general unimodal map of the interval as well.

In addition, the validity of this concept can be extended to higher dimensional maps. A pair of topologically analogous situations is illustrated in Fig. 8 for the two-dimensional case. Beyond the crisis, the unstable manifold of the B saddle intersects the stable manifold of the mediating orbit, the former boundary of the primary basin of attraction, and forms lobes in the S region. The subsequent images of these lobes become elongated along the unstable manifold of the mediating orbit with the rate of its positive Lyapunov exponent. If the system parameter is decreased, the extension of the protruding parts of unstable manifolds decreases proportionally, as in the one-dimensional case discussed above. The combination of this linear change with the geometrical growth of the lobes dictated by the local Lyapunov exponent of the mediating orbit gives the same scaling relation as in the one-dimensional case. This picture obviously remains valid in higher-dimensional maps too, if the mediating orbit is hyperbolic with one unstable direction, and the system's periodic orbits have codimension-1 stable manifolds.

In general, the scaling relation in between two subsequent members of the same family of topologically analogous situations reads as

$$\frac{a_{m+p} - a_c}{a_m - a_c} \approx e^{-p\Lambda}, \quad (14)$$

where p is the period of the mediating orbit. This directly implies the anticipated scaling formulas (8) and, consequently, (7).

The constant coefficient in Eq. (8) is the same for any two members from the same family of topologically analogous situations, but this value varies from one family to the other. As we saw above, topologically analogous situations occur repeatedly beyond the crisis, and their recurrence is periodic in the logarithmic scale with a period determined by the local

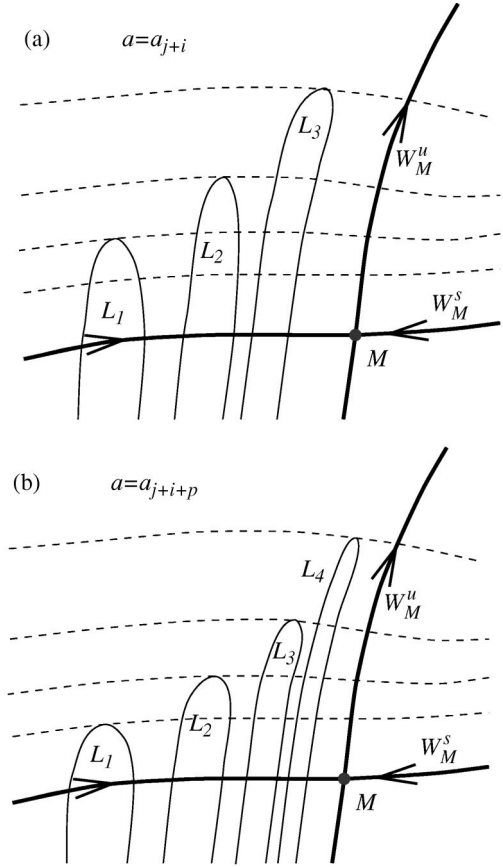


FIG. 8. Schematic illustration of a pair of topologically analogous situations in a dynamical system with two-dimensional phase space. W_M^u and W_M^s denote the unstable and stable manifolds of the mediating orbit M . Dashed lines show the branches of the stable manifold of a remote periodic orbit. Continuous lines show the protruding lobes L_i which, in (a), just have tangencies with that stable manifold at some parameter value $a = a_{j+i}$. In (b), at another parameter value $a = a_{j+i+p}$ closer to the crisis, the lobes have tangencies with the same branches of the same stable manifold, but exactly p iterations later.

Lyapunov exponent of the mediating orbit. Thus the correct asymptotical scaling formula for the minimum length of coupling orbits is

$$m(a) \approx -\frac{\log(a - a_c)}{\Lambda} + \phi[\log(a - a_c) \bmod p\Lambda], \quad (15)$$

where p is the period, Λ is the local Lyapunov exponent of the mediating orbit, and Φ is a periodic function of its argument. This asymptotic scaling formula is universal in the class of systems we defined in the beginning of Sec. II. However, the correction term ϕ , added to the asymptotical trend (7), is not universal: it is a steplike function that jumps at the appropriate a_m values, which is specific to the geometry of the actual crisis situation. The function ϕ involves all the system specific details and determines the *fine structure* of $m(a)$.

C. Topological scaling and other scale invariances

The existence of the periodically recurrent topologically analogous situations is the key structural mechanism that provides the framework for the scaling of other quantities.

Topological arguments referring to similar structures at different system parameter values occur in the decimation step of the renormalization of any scaling quantity, providing principal structural information for the determination of the critical behavior. The existence of topologically analogous situations has already been implicitly used, for example when deriving the scaling behavior of the average burst ratio f in crisis induced intermittency [1] and in finding the critical metric exponent γ of interior crises [7].

Accordingly, we anticipate that the coefficients and correction terms determining the system specific “fine structure” of the scaling quantities are in general *periodic* or *self-similar functions* of the excess parameter of the form

$$F[\log(a - a_c) \bmod p\Lambda], \quad (16)$$

with the periodicity determined by the period p and the local Lyapunov exponent Λ of the mediating orbit. At a given crisis the same periodicity $p\Lambda$ occurs in the scaling formulas of *all* scaling quantities as the signature of the underlying structural scaling phenomenon. The fact that the “fingerprint” of the topological scaling we obtain in this paper appears in the scaling behavior of other quantities emphasizes its *significance and universal character*. (Supporting numerical evidence for this phenomenon can be found, e.g., in Refs. [8,7,15].)

The fine-structure function, of course, has to be determined individually for every quantity and every single crisis situation.

IV. SCALING OF THE TOPOLOGICAL ENTROPY

When the excess parameter $|a - a_c|$ is increased beyond an interior crisis, the minimum period length of the coupling orbits m decreases owing to Eq. (7). This implies the appearance of new, shorter periodic orbits visiting both basic components. This effect, in turn, is reflected in the increase of the topological entropy of the chaotic attractor.

The topological entropy h of a chaotic set [16] is equal to the asymptotic growth rate of $N(n)$, the number of periodic orbits of length n embedded in the chaotic set:

$$h \equiv \lim_{n \rightarrow \infty} [\log N(n)/n]; \quad (17)$$

therefore, in practice the topological entropy is obtained from the asymptotical scaling relation

$$N(n) \sim e^{hn} \quad (18)$$

for $n \rightarrow \infty$.

A. Diagram technique

In what follows, we develop a “diagram technique” to calculate the topological entropy of the enlarged chaotic attractor beyond an internal crisis.

1. Loop number

Note that due to Eq. (15), the system cannot get into the same phase of chaotic motion earlier than $m(a)$ steps at a given parameter a . Therefore, the number of bursts occurring in the course of a long periodic orbit of a given length n can

be at most $\{n/m\}$ (the integer part of n/m). According to this, periodic orbits of length n can be classified and arranged in $\{n/m\} + 1$ classes. There are orbits which never leave or enter region B at all: they correspond to the class $l=0$. Those orbits that escape only once during their period n belong to class $l=1$, the ones that perform exactly two bursts from the class $l=2$, and so on up to $\{n/m\}=l$. We say that an orbit has a *loop number* l , if it belongs to class l .

Let $N_l(n)$ denote the number of orbits of loop number l . Then the topological entropy h of the enlarged attractor—more precisely, that of the whole chaotic set—can be obtained from

$$N(n) = \sum_{l=0}^{\{n/m\}} N_l(n) \sim e^{hn} \quad (19)$$

in the limit $n \rightarrow \infty$.

2. Propagators

Let the diagrams introduced in Eq. (12) for the quadratic map (4) henceforth represent the number of different itineraries (of a given length j) allowed by the dynamics on the basic component belonging to the respective phase in a general system. This number increases with the length j according to the partial topological entropies of the respective basic components:

$$\text{=====} \sim e^{h^{[B]}j} \equiv b^j, \quad (20a)$$

$$\text{-----} \sim e^{h^{[S]}j} \equiv s^j, \quad (20b)$$

$$\text{.....} \sim e^{h^{[M]}j} \equiv c^j \equiv 1. \quad (20c)$$

Note that in Eq. (20c) $c=1$ and the corresponding topological entropy $h^{[M]}$ is 0, reflecting the fact that during the intermittent phase the trajectories, stay in the vicinity and follow the motion of the same mediating orbit. (If the system has a generating partition, we can say they follow a fixed itinerary.)

We can consider b , s , and c as *propagators* denoting the contribution of the three phases of crisis induced intermittent motion. In addition, we also introduce a global propagator t , and a diagram to represent the contribution of arbitrary allowed sequences of length j :

$$\text{—————} \sim e^{hj} \equiv t^j. \quad (21)$$

Obviously, the growth rate of this sort of sequence is determined by the overall topological entropy h of the whole chaotic set.

We suppose that the topological entropy $h = \log t$ of the whole chaotic set is somewhat larger than $h^{[S]} = \ln s$. Owing to these, the relations

$$t \geq s > b > c \Rightarrow t^n > s^n \gg b^n \gg c^n \quad (22)$$

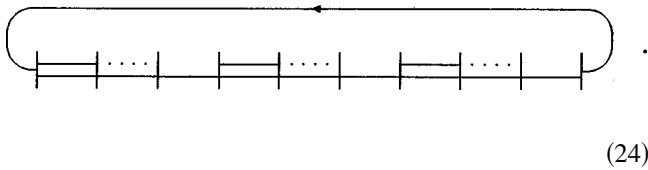
are held among the growth rates.

3. Cyclic diagrams

By combining the above diagrams, we can describe the patterns of subsequent phases of the motion. Obviously, periodic orbits of the dynamics periodically repeat their pattern; we can illustrate this fact by symbolically connecting the end and the beginning of the row of propagators, like



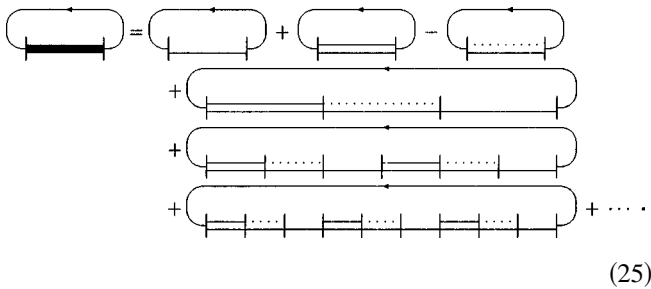
and



These *cyclic diagrams* then represent the number of periodic orbits of length n that fit to the pattern prescribed by the sequence of propagators. For example, diagram (23) represents $N(n)$, the total number of all allowed periodic orbits, while diagram (24) denotes $N_3(n)$, the number of loop number 3 periodic orbits.

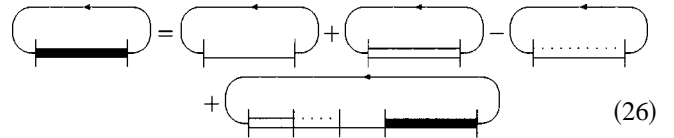
4. Diagram equations

By using the above diagrams, expression (19) is equivalent to the following diagram equation:



Recall that the mediating orbit belongs to both basic components; thus it is taken into account twice (in the first two diagrams) on the right hand side. To correct this, its contribution must be subtracted in the third term. In addition to these loop number 0 terms, the contribution of each further class of loop number l orbits is represented by a single diagram in increasing loop order. In the Appendix we actually calculate some of these diagrams for given finite n values.

The topological entropy need to be determined in the limit $n \rightarrow \infty$, when the sum in Eq. (19) becomes an infinite series. Taking this limit in Eq. (25) yields the self consistent diagram equation



which is formally similar to that of Dyson's equation. Note that in this formula the contributions of the basic components and of the heteroclinic component appear *separately* from each other.

In the Appendix, we give a self consistent solution of Eq. (26). The calculation uses the relations (22) among the propagators, and eventually yields

$$t \approx s(1 + Cs^{-m}), \tag{27}$$

for the propagator t , where C is a parameter dependent coefficient of the universal form (16). Taking the logarithm gives

$$h \approx h^{[S]} + \log(1 + Ce^{-h^{[S]}m}), \tag{28}$$

for the topological entropy of the whole chaotic set, which close to the crisis (i.e., at $m \gg 1$) reads as

$$h \approx h^{[S]} + Ce^{-h^{[S]}m}. \tag{29}$$

B. Topological entropy as a function of the system parameter

As $a \rightarrow a_c$, the minimum loop length m diverges [cf. Eq. (15)] and the topological entropy of the whole chaotic set approaches $h^{[S]}$ in the critical limit:

$$h_c \equiv h(a_c + 0) = h^{[S]}. \tag{30}$$

Since the basic component in the surrounding region S is structurally stable, the value of its topological entropy $h^{[S]}$ remains unchanged in the postcritical regime $a > a_c$. The explicit parameter dependence can be obtained by combining the exponential expression (29) with the logarithmic scaling formula (15) found for the minimum period length of the coupling orbits. The topological entropy depends on a only through m and C , both of them follow form (16). This yields the *scaling relation*

$$h(a) - h_c \approx \psi[\log(a - a_c) \bmod p\Lambda](a - a_c)^\chi, \tag{31}$$

with the critical exponent

$$\chi = \frac{h_c}{\Lambda}. \tag{32}$$

This formula gives the parameter dependence of the *excess topological entropy*. This quantity characterizes the *development of the heteroclinic component* beyond the crisis point.

It is worth emphasizing that the critical exponent depends on the local Lyapunov exponent of the mediating periodic orbit (Λ) and on the topological entropy ($h^{[S]}$) of the basic component in the S region only. Therefore, one can say that the critical exponent of the topological entropy is determined exclusively by the *local* properties of the *mediating orbit* and the *global* behavior of one of the basic components: the *pre-critical saddle*. The other basic component, i.e., that of the

precritical attractor, does not influence the trend of topological development of the enlarged attractor in the postcritical regime. Note that in the above self consistent calculation every system specific (and periodic window specific) detail is condensed in the factor ψ .

In the course of the development of the scaling relation (31) we took advantage of the following three assumptions only: (i) the crisis induced intermittent behavior beyond crisis follows scheme (3); (ii) the minimum length of the intermittent phase in the vicinity of the mediating orbit diverges according to Eq. (15); and (iii) the separation of the basic components' topological entropies, i.e., relation (22), holds. We have argued that these conditions are generally fulfilled at typical attractor enlargement crises, *even in higher-dimensional maps*, if the chaotic sets have only one unstable dimension. Therefore we claim that *the scaling formula (31) for the topological entropy holds for the entire class* of such chaotic maps. The correct critical exponent χ in such cases is always given by substituting the appropriate values of the largest topological entropy of the two basic components and the local Lyapunov exponent of the mediating orbit in Eq. (32). (See the remarks in Appendix A 3.)

We would like to emphasize here the difference between the topological entropy of the attractor and the topological entropy of the whole chaotic set. First, consider a precritical situation within the periodic window. On the one hand, there are no coupling orbits present in the system, and thus only the first two diagrams appear on the right hand side of Eqs. (25) and (26). Relation (22) yields that the topological entropy of the whole chaotic set is $h = \log(s) = h^{[S]}$, the greater of the two basic component's topological entropy. On the other hand, the topological entropy of the attractor is obviously $\log(b) = h^{[B]}$. By also taking Eq. (30) into account, we can conclude that the topological entropy of the attractor undergoes a jump from $h^{[B]}$ to $h^{[S]}$ at a_c , while the topological entropy of the whole chaotic set is continuous at the crisis point. The situation is similar at the starting point(s) a_b and a_c of the periodic window (cf. Fig. 1). Consequently, the topological entropy of the whole chaotic set changes continuously as the parameter varies through the periodic window, while the topological entropy of the attractor shows a sudden change at both ends of the periodic window. These discontinuities can be observed as a signature of crisis [17]. However they reflect only a change in the asymptotic stability of a basic component, rather than any abrupt structural change in the overall invariant set.

Note that very small periodic orbits with high periods also occur in the postcritical regime $a > a_c$. According to the above arguments, the topological entropy of the whole chaotic invariant set, for which the scaling formula (31) has been developed in this section, changes continuously through these windows. This implies that the fine structure function ψ in Eq. (31) is a continuous function of the system parameter.

V. NUMERICAL TESTS

In this section we briefly summarize the numerical procedures we carried out to verify scaling relation (1). Here we present the results we obtained for the interior crises of the two example maps discussed earlier.

First we consider the interior crisis of the quadratic map

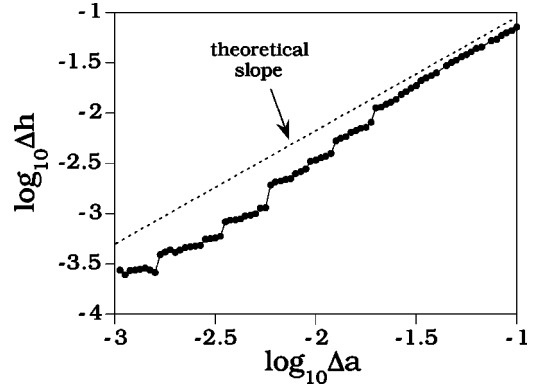


FIG. 9. Numerically obtained scaling of the excess topological entropy in the quadratic map (4). The straight line represents a line with the theoretical slope 1.1.

(4) discussed in Secs. II B and III A. The Lyapunov exponent of the mediating period 3 orbit at a_c is $\Lambda \approx 0.437452$. h_c , the topological entropy of the repeller in region S , is known exactly from Eq. (5). This yields $\chi = \log(h^{[S]})/\Lambda \approx 1.1$ for the predicted value of the scaling exponent (32).

In order to verify the scaling relation (1), we computed the topological entropy in a small parameter interval $[a_c + 10^{-4}, a_c + 10^{-1}]$ beyond the crisis, at 120 parameter values of $\Delta a = a - a_c$ uniformly distributed on the logarithmic scale. At each parameter value we determined the corresponding topological entropy of the attractor from a logarithmic fit to Eq. (18), where the $N(n)$ values were determined from the map's known symbolic dynamics for $1 < n \leq 18$ long symbol strings. The numerically obtained values for $h(a)$ of course involve some error; in our case the confidence interval for the estimated values of h was about 10^{-3} . The error bar on $h(a)$ imposes a strict lower limit for the $\Delta h = h(a) - h_c$ values one can sensibly test against the expected scaling behavior (1). This, in turn, sets a lower limit for Δa values as well: in our case, according to Fig. 9, the theoretically predicted scaling law (1) can only be verified for $\Delta a \gg 10^{-3}$ above a_c . Figure 9 indicates that the agreement between numerics and theory with this constraint obeyed is good.

As we see, the limiting factor in determining the scaling exponent χ in Eq. (1) is the available precision in the calculation of the topological entropy. A reliable computation of the topological entropy is highly nontrivial in higher dimensional chaotic systems. We have found that the method of Newhouse and Pignataro [18] appears to give the most reliable estimation of the topological entropy for our particular purpose among other methods we have tried.

In the study of the interior crisis of the Hénon map (6), discussed in Sec. II C, we followed a similar procedure to the quadratic equation's case. However, we used the Newhouse-Pignataro method [18] instead of symbolic dynamics, and $h_c \approx 0.38$ also had to be determined numerically. The largest eigenvalue of the period-7 mediating orbit was found to be approximately $10.87^{1/7}$, corresponding to $\Lambda \approx 0.341$ and $\chi \approx 1.12$. Despite the serious limitations imposed by the available precision of the topological entropy's calculation, we managed to confirm the corresponding expected value of the exponent by the numerically obtained value (1.13 ± 0.11), as shown in Fig. 10. (For further details, see Ref. [4].)

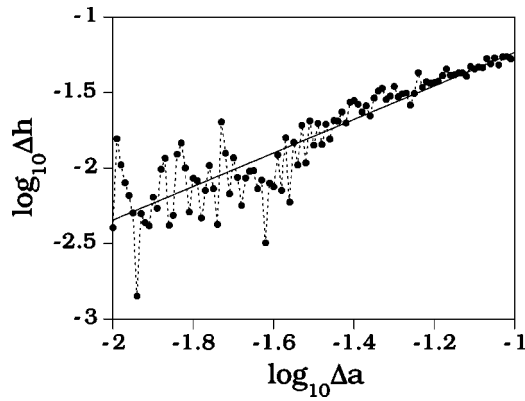


FIG. 10. Scaling of the excess topological entropy near the crisis of the Hénon map. The straight line fit corresponds to the numerical gap filling exponent $\chi = 1.13 \pm 0.11$, which agrees with the theoretical prediction $\chi \approx 1.12$.

VI. DISCUSSION

In this work we gave a detailed explanation of the *gap filling* phenomenon that accompanies interior crises in chaotic dynamical systems. We have obtained a scaling law governing the change of the topological entropy accompanying the gap filling with a new *fundamental scaling exponent* as a characteristic quantity of the gap filling phenomenon. The scaling law (1) establishes a relationship between the abrupt change at crisis and the subsequent quasicontinuous structural development. The essence of the diagram technique we presented here is a systematic account taking of the interactions among the *basic dynamical components* involved in the interior crisis. Our arguments and the diagram equations are general enough to hold regardless of the details of the system. Therefore, the scaling law for gap filling is valid for the *attractor explosion* [19,20,7,15,21–25,13] crises of a wide class of chaotic systems, including higher-dimensional maps. We also expect that the method is generally applicable for investigating phenomena which involve the interaction of two or more invariant sets and the scalings of other quantities.

Attractor merging [26–28,1] is a similar phenomenon when two or more disjoint coexisting attractors become parts of an enlarged attractor. If the system has certain symmetries, interior crisis might also occur in the form of *symmetry recovering attractor merging* [1,26], for which case scheme (3) describing the pattern of crisis induced intermittency can be further modified so as to accommodate the intermittent phases preceding the switches in both directions:

$$\begin{aligned}
 (\text{chaos})_1 &\rightarrow (\text{approximately periodic})_i \rightarrow (\text{chaos})_2 \\
 &\rightarrow (\text{approximately periodic})_{ii} \rightarrow (\text{chaos})_1 \\
 &\rightarrow (\text{approximately periodic})_i \rightarrow (\text{chaos})_2 \\
 &\rightarrow (\text{approximately periodic})_{ii} \rightarrow (\text{chaos})_1 \rightarrow \dots
 \end{aligned} \tag{33}$$

Here $(\text{chaos})_1$ and $(\text{chaos})_2$ represent the two types of chaotic motion on the merged attractor, associated with a symmetric pair of basic nonattracting chaotic sets. The calculation in this case can make use of the symmetry, namely, that

phases 1 and 2 of the motion have the same partial topological entropies. The approximately periodic behaviors i and ii can occur in the vicinity of the *same* mediating orbit if it is of odd symmetry.

In the case of a *double interior crisis* where two crises occur simultaneously as two parameters are varied [29], two different intermittent (e.g., transient) chaotic signals occur in the system, both of them correspond to a basic component. In such a system instead of a mediating periodic orbit, a third chaotic saddle may reside on the boundary in between the two chaotic bands. Then the qualitative dynamical picture is

$$\begin{aligned}
 (\text{chaos})_1 &\rightarrow (\text{chaos})_{\text{FBB}} \rightarrow (\text{chaos})_2 \rightarrow (\text{chaos})_{\text{FBB}} \rightarrow (\text{chaos})_1 \\
 &\rightarrow (\text{chaos})_{\text{FBB}} \rightarrow (\text{chaos})_2 \rightarrow (\text{chaos})_{\text{FBB}} \rightarrow (\text{chaos})_1 \\
 &\rightarrow \dots
 \end{aligned} \tag{34}$$

where both chaotic phases are followed by a third type of *chaotic motion*, $(\text{chaos})_{\text{FBB}}$, on the fractal basin boundary (FBB). In such cases renormalization should be done with (at least) two accessible system parameters simultaneously: this problem is open to further investigation.

In addition to gap filling, an alternative mechanism of structural development, *pruning*, also occurs in chaotic systems where the basic source of nonlinearity is a *discontinuity*. For such systems a scaling formula for the *decrease* of the topological entropy similar to Eq. (1) was derived with a different exponent in Ref. [30].

Most characteristic scaling quantities of chaotic behavior (like generalized dimensions, Rényi entropies, Lyapunov exponents, and escape rate) can be related to formal partition sums [31]. The topological entropy and the associated partition sum (19) are the simplest examples for such a description. At crises such quantities undergo drastic changes that are analogous to phase transitions. Such transitions are also related to the interaction of the system's basic components [6,10]. The approach we elaborated in this paper for the topological entropy is general enough to be applicable to other types of partition sums. By associating appropriate meaning and values to the propagators (20) and coupling constants, the diagram technique introduced here may provide a suitable apparatus for studying and solving the critical behavior of other scaling quantities around crises as well.

ACKNOWLEDGMENTS

This work was supported by the U.S.–Hungary Science and Technology Program (JF Grant Nos. 286 and 501) and by the Hungarian National Science Foundation (OTKA F17166, T17493, and T19483). Y.C.L. was supported by AFOSR under Grant No. F49620-98-1-0400, by NSF under Grant No. PHY-9722156. C.G. was supported by DOE (Mathematical, Information, Computation Science Division, High Performance Computing and Communication Program) and by an CNP_q/NSF joint grant. One of the authors (K.G.Sz.) is indebted to the faculty of the Mathematics Department of the University of Kansas for their kind hospitality.

APPENDIX: SOLVING THE DIAGRAM EQUATIONS

In Sec. IV A we set up a symbolic diagram formalism to estimate the topological entropy via Eq. (19). In this appendix, we first investigate the terms in Eq. (25) in increasing loop order by using the propagators defined in Eqs. (20) and (21). Then we solve the diagram equation (26), and derive the formula (28) of the excess topological entropy beyond the critical parameter value a_c .

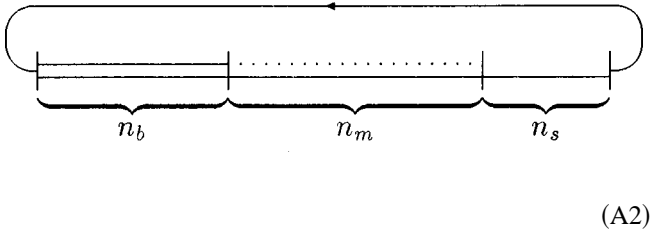
1. Cyclic diagrams

a. Loop number 0. Consider the three diagrams shown in Eq. (20). The first two diagrams take into account the orbits that never leave regions B and S , respectively: they represent the periodic orbits belonging to the two basic components. The number of these orbits increases with the rate determined by the topological entropies of the basic components [cf. Eq. (20)]. Recall that the mediating orbit belongs to both basic components; therefore, we have to *subtract* its contribution to obtain the zeroth order term in Eq. (19):

$$N_0(n) \sim s^n + b^n - c^n \approx s^n. \quad (\text{A1})$$

The asymptotic behavior on the right hand side follows from Eq. (22). The resulting growth rate in this loop order is $\log s$, i.e., $h^{[S]}$.

b. First loop order. The number of periodic orbits of length n that visits both regions *exactly once* is denoted by the diagram



In the example of the period-3 window of the quadratic map (4) each trajectory must spend at least one time step within B_1 after escaping region S and before leaving B again [cf. Sec. III A, Figs. 2 and 5]. Therefore in this case $n_b \geq 1$ and the intermittent phase close to the mediating orbit must last for at least $m-1$ steps. In a general system the topology may determine that a trajectory must spend at least j_B steps in B before an intermittent phase, and at least j_S steps in S after it. (Obviously $j_B < p$, and j_S is also expected to be a very small number.) This implies that the minimum length of the intermittent phase with fixed itinerary close to M is $m - j_B - j_S$. Thus the length of the individual phases in diagram (A2) must satisfy the relations $n_b \geq j_B$, $n_s \geq j_S$, and $n_m \geq m - j_B - j_S$. Taking into account that the total length of the orbits is $n = n_b + n_m + n_s$, the number of orbits with loop number 1 can be calculated as

$$\begin{aligned} N_1(n) &= \xi \sum_{n_b=j_B}^{n-m+j_B} \sum_{n_m=m-j_B-j_S}^{n-n_b-j_S} b^{n_b} c^{n_m} s^{n-n_b-n_m} \\ &= \xi (b/c)^{j_B} (s/c)^{j_S} c^m \\ &\quad \times \frac{s^2(b-c)s^{n-m} + b^2(c-s)b^{n-m} + c^2(s-b)c^{n-m}}{(s-b)(b-c)(s-c)} \\ &= Cc^m [s^{n-m} + Bb^{n-m} + Ac^{n-m}] \end{aligned} \quad (\text{A3a})$$

$$\approx Cc^m s^{-m} s^n, \quad (\text{A3b})$$

where

$$A = b^2(c-s)/(b-c) \quad \text{and} \quad B = c^2(s-b)/(b-c) \quad (\text{A4})$$

are the constant coefficients. The *loop coupling factor*

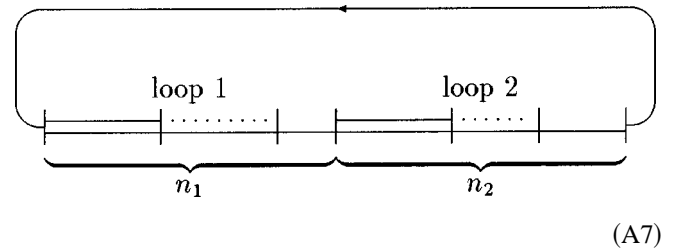
$$C = \frac{s^2}{(s-b)(s-c)} (b/c)^{j_B} (s/c)^{j_S} \xi \quad (\text{A5})$$

contains a generic part, a topology dependent part (j_B and j_S are fixed for a given window), and a system parameter dependent factor ξ . The latter factor measures the proportion of how many closed orbits are actually realized among those of the mere combinations of paths allowed by the dynamics of the individual phases. (An orbit of length n is realized whenever the return condition $y_n = y_0$ can be fulfilled for some $y_0 \in B$.) Asymptotically, ξ is identical within a family of topologically analogous situations, which implies the system parameter dependence

$$\xi = \xi[\log(a - a_c) \bmod p\Lambda] \quad (\text{A6})$$

as outlined in Sec. III C. This property implies that the loop coupling factor in Eq. (A5) has a similar a -dependence. ξ also incorporates the constant factors not shown in the scaling relations (20) and (21). Note that the growth rate obtained from the asymptotical behavior (A3b) does not exceed the critical value $h^{[S]}$.

c. Second loop order. In the second loop order we consider the number of orbits fitting to the graph



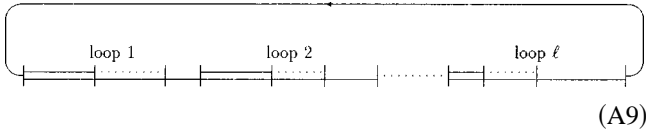
where both phases are at least m steps long and $n = n_1 + n_2$. These orbits can be combined from two first loop number orbits. The number of such combinations can be obtained as

$$\begin{aligned}
N_2(n) &= \xi_2 \frac{1}{2} \sum_{n_1=m}^{n-m} N_1(n_1)N_1(n-n_1) \\
&= \xi_2 \frac{1}{2} \sum_{n_1=m}^{n-m} C^2 c^{2m} (s^{n_1-m} + Bb^{n_1-m} + Ac^{n_1-m}) \\
&\quad \times (s^{n-n_1-m} + Bb^{n-n_1-m} + Ac^{n-n_1-m}) \\
&\approx \xi_2 \frac{n+1-2m}{2} [Cc^m s^{-m}]^2 s^n \quad (\text{A8})
\end{aligned}$$

by using formula (A3a) and taking the asymptotic limit $n \rightarrow \infty$. Here the factor ξ_2 plays a role similar to ξ in Eq. (A3), and it also takes the same sort of parameter dependence.

Due to the n -dependent first factor, this term increases somewhat faster than s^n ; however the contribution of this term to the growth rate is of the order of $\log(n)/n$, which disappears in the asymptotic limit.

d. Higher order loops. In the subsequent loop orders the diagrams



represent

$$\begin{aligned}
N_l(n) &= \xi_l \frac{1}{l} \sum_{n_1=m}^{n-m} N_1(n_1)N_{l-1}(n-n_1) \\
&\approx \xi_l \frac{(n+1-lm)^{l-1}}{l!} [Cc^m s^{-m}]^l s^n \quad (\text{A10})
\end{aligned}$$

new orbits. The number of the repeated combinations of the allowed one-loop itineraries is divided by l in order to exclude the cyclic permutation of identical patterns.

Despite the gradual increase in the n -dependent combinatorial prefactor with increasing loop number l , the asymptotical growth rate in each order remains $\log s$. However, the infinite sum (19) grows faster than s^n in the $n \rightarrow \infty$ limit. This fact shows, on the one hand, that *the cause of the excess topological entropy beyond crisis is basically the increased combinatorial possibility of the two sorts of chaotic transients*; on the other hand, that gap filling phenomenon is associated with the appearance of *extremely long coupling orbits*. Note that by decreasing m , the correction terms grow rapidly.

2. Solution of the self consistent equation

In order to obtain the asymptotic value of the excess topological entropy, we perform a self consistent calculation below. Let us suppose that the number of periodic orbits of the attractor, symbolized by the propagator (21), increases as

$$N(n) \approx D \cdot t^n \equiv D \cdot e^{hn}, \quad (\text{A11})$$

where D is an arbitrary factor of order 1. We also use that the topological entropy $h = \log t$ is somewhat greater than $h^{[S]}$

$= \log s$, in accordance with relations (22) among the growth rates. The diagram equation (26) can be written as

$$N(n) = N_0(n) + \xi_\infty \sum_{n_1=m}^n N_1(n_1)N(n-n_1), \quad (\text{A12})$$

where ξ_∞ has similar meaning and parameter dependence to that of ξ in Eq. (A6). By substituting the expressions (A11), (A1), and (A3a) into Eq. (A12), we find that

$$\begin{aligned}
Dt^n &\approx s_0 s^n + b_0 b^n - c_0 c^n + \xi_\infty \\
&\quad \times \sum_{n_1=m}^n Cc^m (s^{n_1-m} + Bb^{n_1-m} + Ac^{n-m}) Dt^{n-n_1} \\
&= s_0 s^n + b_0 b^n - c_0 c^n + \xi_\infty \\
&\quad \times Cc^m Dt^{n-m} \sum_{j=0}^{n-m} \left[\left(\frac{s}{t}\right)^j + B \left(\frac{b}{t}\right)^j + A \left(\frac{c}{t}\right)^j \right] \\
&= s_0 s^n + b_0 b^n - c_0 c^n + Dt^n \xi_\infty Cc^m t^{-m} \\
&\quad \times \left[\frac{1 - (s/t)^{n+1-m}}{1 - (s/t)} + B \frac{1 - (b/t)^{n+1-m}}{1 - (b/t)} \right. \\
&\quad \left. + A \frac{1 - (c/t)^{n+1-m}}{1 - (c/t)} \right], \quad (\text{A13})
\end{aligned}$$

where s_0 , b_0 , and c_0 are constants, assumed but not shown in the asymptotical scaling relation (20). The coefficients A , B , and C are the same as given in Eqs. (A4) and (A5) for the loop number 1 orbits. However, without loss of generality, we can incorporate ξ_∞ in ξ and, consequently, in C as well [cf. Eq. (A5)]. Then, by dividing by the leading order term Dt^n and taking the limit $n \rightarrow \infty$, one can eliminate the vanishing terms due to Eq. (22), and obtain the following implicit equation for t :

$$\begin{aligned}
1 &= Cc^m t^{1-m} \left(\frac{1}{t-s} + \frac{B}{t-b} + \frac{A}{t-c} \right) + \left(\frac{s_0}{D} - \frac{Cc^m s^{l-m}}{t-s} \right) \left(\frac{s}{t} \right)^n \\
&\quad + \left(\frac{b_0}{D} - B \frac{Cc^m b^{1-m}}{t-b} \right) \left(\frac{b}{t} \right)^n + \left(-\frac{c_0}{D} - A \frac{Cc}{t-c} \right) \left(\frac{c}{t} \right)^n \\
&\approx Cc^m t^{1-m} \left(\frac{1}{t-s} + \frac{B}{t-b} + \frac{A}{t-c} \right). \quad (\text{A14})
\end{aligned}$$

Therefore, for any given parameter value a , the asymptotic equation for t is a polynomial equation of degree $m+2$:

$$\begin{aligned}
F(t) &= t^{m-1}(t-s)(t-b)(t-c) - Cc^m \\
&\quad \times \{(t-b)(t-c) + (t-s)\} \\
&\quad \times [B(t-c) + A(t-b)] = 0. \quad (\text{A15})
\end{aligned}$$

For parameter values close to the crisis point a_c , i.e., for $m \gg 1$, the three greatest roots of this polynomial are close to s , b , and c . Moreover, $F(t)$ becomes very steep around s ,

whereupon it follows that the greatest root of Eq. (A15) can be well approximated via linear expansion around s :

$$0 = F(t) \approx F(s) + F'(s)(t-s) \quad (\text{A16})$$

From the above expansion,

$$t \approx s - \frac{F(s)}{F'(s)} = s + \frac{Cc^m(s-b)(s-c)}{s^{m-1}(s-b)(s-c) - Cc^m[(A+1)(s-b) + (B+1)(s-c)]} \approx s[1 + Cc^m s^{-m} + \mathcal{O}(Cc^m s^{-m})^2] \quad (\text{A17})$$

follows for the greatest root of Eq. (A15).

Taking the logarithm, according to Eq. (A11), yields the topological entropy of the whole attractor as

$$h \approx h^{[S]} + \log[1 + Ce^{(h^{[M]} - h^{[S]})m}]. \quad (\text{A18})$$

By taking $m \gg 1$ into consideration again,

$$h - h^{[S]} \approx Ce^{(h^{[M]} - h^{[S]})m} \quad (\text{A19})$$

follows for the excess topological entropy, reflecting the increasing number of coupling orbits above the critical point.

The coefficient C in Eqs. (A17)–(A19) inherits a system parameter dependence from ξ via Eqs. (A5) and (A6), and follows the general form (16) of fine structure functions. This provides the same coefficient for the members of a given family of topologically analogous situations in the scaling equation (A19), but different values for different families.

3. Remarks

(1) Equations (27)–(29) in Sec. IV directly follow from Eqs. (A17)–(A19) by using the conditions $c=1$ and $h^{[M]} = 0$ given for the propagator and the topological entropy of

the mediating periodic orbit in Eq. (20). In this appendix we did not use this condition in order to keep our calculation valid for cases where the mediating invariant set is a chaotic saddle rather than a periodic orbit, i.e., if the basic components have a *fractal basin boundary*. (See Sec. VI for implications in other types of crises.)

(2) The separation of the topological entropies (22) is the basic condition for the validity of our derivation. However, if in some unusual case the separation scheme

$$t \geq b > s > c \Rightarrow t^n > b^n \gg s^n \gg c^n \quad (\text{A20})$$

holds instead of Eq. (22), the scaling formula (31) remains valid. In this case the calculations of this appendix can be carried out with the role of the two basic components exchanged, and the substitutions

$$b \leftrightarrow s, \quad C \rightarrow \hat{C} \equiv \frac{b^2(c-s)}{s^2(b-c)} C \quad \text{and} \quad h_c \equiv h^{[B]} \quad (\text{A21})$$

yield the correct values in the appropriate formulas Eqs. (27)–(30) of Sec. IV. Note that h_c , the critical value of the topological entropy is always the maximum of the two basic components' topological entropies.

-
- [1] C. Grebogi, E. Ott, and J. A. Yorke, *Physica D* **7**, 181 (1983).
 [2] C. Jeffries and J. Perez, *Phys. Rev. A* **27**, 601 (1983); S. D. Brorson, D. Dewey, and P. S. Linsay, *ibid.* **28**, 1201 (1983); H. Ikezi, J. S. DeGrasse, and T. H. Jensen, *ibid.* **28**, 1207 (1983); A. R. W. Rollins and E. R. Hunt, *ibid.* **29**, 3327 (1984); M. Iansiti *et al.*, *Phys. Rev. Lett.* **55**, 746 (1985); D. Dangoisse, P. Glorieux, and D. Hennequin, *ibid.* **57**, 2657 (1986); W. L. Ditto *et al.*, *ibid.* **63**, 923 (1989); R. Stoop and J. Parisi, *Phys. Rev. A* **43**, 1802 (1991); J. C. Sommerer *et al.*, *Phys. Rev. Lett.* **66**, 1947 (1991); *Phys. Lett. A* **153**, 105 (1991); J. C. Sartorelli, W. M. Gonçalves and R. D. Pinto, *Phys. Rev. E* **49**, 3963 (1994); I. M. Kyprunidis *et al.*, *ibid.* **52**, 2268 (1995).
 [3] I. M. Jánosi, L. Flepp, and T. Tél, *Phys. Rev. Lett.* **73**, 529 (1994).
 [4] K. G. Szabó, Y.-C. Lai, T. Tél, and C. Grebogi, *Phys. Rev. Lett.* **77**, 3102 (1996).
 [5] T. Y. Li and J. A. Yorke, *Am. Math. Monthly* **82**, 985 (1975).
 [6] K. G. Szabó and T. Tél, *Phys. Lett. A* **196**, 173 (1994).
 [7] C. Grebogi, E. Ott, F. Romeiras, and J. A. Yorke, *Phys. Rev. A* **36**, 5365 (1987).
 [8] C. Grebogi, E. Ott, and J. A. Yorke, *Phys. Rev. Lett.* **48**, 1507 (1982).
 [9] Bai-lin Hao, *Experimental Study and Characterization of Chaos* (World Scientific, Singapore, 1990).
 [10] K. G. Szabó and T. Tél, *Phys. Rev. E* **50**, 1070 (1994).
 [11] M. Hénon, *Commun. Math. Phys.* **50**, 69 (1976); M. Benedicks and L. Carleson, *Ann. Math.* **133**, 73 (1991).
 [12] R. W. Leven and M. Selent, *Chaos Solitons Fractals* **4**, 2217 (1994).
 [13] Y. C. Lai, C. Grebogi, and J. A. Yorke, in *Applied Chaos*, edited by J. H. Kim and J. Stringer (Wiley, New York, 1992), p. 441.
 [14] The superstability points themselves are special Misiurewicz points.
 [15] B. Pompe and R. W. Leven, *Phys. Scr.* **38**, 651 (1988).
 [16] R. C. Adler, A. C. Konheim, and M. H. McAndrew, *Trans. Am. Math. Soc.* **114**, 309 (1965).
 [17] Y. S. Fan and T. R. Chay, *Phys. Rev. E* **51**, 1012 (1995).
 [18] S. Newhouse and T. Pignataro, *J. Stat. Phys.* **72**, 1331 (1993).
 [19] R. W. Leven and B. P. Koch, *Phys. Lett.* **86A**, 71 (1981).
 [20] C. Grebogi, E. Ott, and J. A. Yorke, *Phys. Rev. Lett.* **57**, 1284 (1986).
 [21] K. Tomita *et al.*, *Prog. Theor. Phys.* **80**, 953 (1988); **81**, 1124 (1989).
 [22] J. C. Sommerer, E. Ott, and C. Grebogi, *Phys. Rev. A* **43**, 1754 (1991).

- [23] H. Shibata, H. Fujisaka, and H. Mori, Phys. Lett. A **189**, 554 (1992).
- [24] M. Franaszek and A. Nabaglo, Phys. Lett. A **178**, 85 (1993); **182**, 99 (1993); M. Franaszek, Phys. Rev. A **46**, 6340 (1992).
- [25] R. W. Leven, M. Selent, and D. Uhrlandt, Chaos Solitons Fractals **4**, 661 (1994).
- [26] H. Fujisaka, H. Kamifukumoto, and M. Inoue, Prog. Theor. Phys. **69**, 333 (1993); F. T. Arecchi, R. Badii, and A. Politi, Phys. Lett. **103A**, 3 (1984); K. Aoki, O. Ikezawa, and H. Kamifukumoto, *ibid.* **106A**, 343 (1984); H. Ishii, H. Fujisaka, and M. Inoue, Phys. Lett. A **116**, 257 (1986); H. Uchimura, H. Fujisaka, and M. Inoue, Prog. Theor. Phys. **77**, 1344 (1987).
- [27] T. Horita *et al.*, Prog. Theor. Phys. **80**, 793 (1988).
- [28] N. Platt, E. A. Spiegel, and C. Tresser, Phys. Rev. Lett. **70**, 279 (1993).
- [29] J. A. Gallas, C. Grebogi, and J. A. Yorke, Phys. Rev. Lett. **71**, 1359 (1993).
- [30] J. Vollmer and W. Breyman, Europhys. Lett. **27**, 23 (1994).
- [31] J.-P. Eckmann and D. Ruelle, Rev. Mod. Phys. **57**, 617 (1985); C. Beck and F. Schlögl, *Thermodynamics of Chaotic Systems—An Introduction* (Cambridge University Press, Cambridge, England, 1993).